

# Performance of SnSb:Ce, Co alloy as anode for lithium-ion batteries

D. Lakshmi<sup>1</sup> · B. Nalini<sup>1</sup>

Received: 23 July 2016 / Revised: 24 October 2016 / Accepted: 28 October 2016 / Published online: 9 November 2016  
© Springer-Verlag Berlin Heidelberg 2016

**Abstract** Synthesis of pure tin-antimony (SnSb) by co-precipitation method using metal chlorides as starting materials and Ce, Co-incorporated SnSb is reported and examined. The structure of the doped SnSb is compared with the pure SnSb by means of XRD analysis in which no structural variation is observed. Strain analysis is carried out by Williamson-Hall (WH) plot method. Compared to the intact SnSb, diminutive decrement in unit cell volume is observed for the doped SnSb, which indicates the rigidity of the structure after doping. The electrochemical properties are analyzed by cyclic voltammetry, electrochemical impedance spectroscopy, and reversibility testing. Improved redox activity and reversibility are observed for SnSb:Ce, Co anode due to the well-resolved grain and grain boundary regions. Doped anode exhibits specific capacitance around  $319 \text{ Fg}^{-1}$  for 50 cycles. The augmented capacity and electrical conductivity of the SnSb:Ce, Co anode will enhance the rate capability of it, and this makes SnSb:Ce, Co a promising anode material for solid-state lithium-ion batteries in energy systems.

**Keywords** Tin-antimony alloy · Anode · Co-precipitation · Specific capacitance · Lithium-Ion battery

## Introduction

Lithium-ion batteries (LIBs) are considered as the most promising energy storage technologies for cellular phones,

notebook PCs, and electric vehicles. Increasing the energy density of the Li-ion batteries is necessary to use them in higher-energy applications such as hybrid electric vehicles [1]. Commercially used carbon-based anode materials possess very low energy density and poor theoretical capacities [2–4]. In order to enhance the energy density of the electrode material, intermetallic anodes are being analyzed. Tin-based anodes are found to possess higher theoretical capacity and more lithium uptake [ $\text{Li}_{22}\text{Sn}_5$ –994  $\text{mAh g}^{-1}$ ] compared to the carbon-based materials. Despite of high theoretical capacity of these types of anodes, they undergo severe structural instability during alloying/de-alloying process of Li ions, which leads to poor cyclability of the battery and hence minimized lifetime [5–8].

The range of speculations to heighten the stability of these types of conversion anodes are by preparing composites with carbon or other metal dopants [9–11]. An effective approach is employing active/inactive metal dopants, which are shown with distinctive illustrations [6, 12–26]. However, these approaches have shown only limited enhancement. The inactive metal dopants can enhance the electrical properties of the tin-based alloy anodes by providing a flexible matrix for lithiation and de-lithiation process to hinder the structure of the electrode from volumetric changes [27, 28]. Among various dopants, Fe-doped tin-antimony (SnSb) alloys deliver high theoretical capacity compared to the other metal additives in the SnSb matrix. Cobalt-doped Sn anode has been reported by other researchers [29], which was found to exhibit improved cycling performance. However, Sn-Co anode delivered low capacity compared to the Fe-based SnSb matrix [30].

In this work, Ce, a rare earth metal element, and Co, a transition metal element, have been co-doped in the tin-antimony system to enhance the cyclability of the SnSb anode. Being inactive dopants, Ce and Co do not show any additional redox activity in the tin-antimony system; still, they improve

✉ B. Nalini  
jyothsnalalin99@gmail.com

<sup>1</sup> Department of Physics, Avinashilingam Institute for Home Science and Higher Education for Women University, Coimbatore, India

cyclability of the anode. Besides, the dopants in the SnSb matrix not only provide structural stability but also increase the electronic conductivity of the matrix. Such an augmentation in electronic conductivity favors the high rate performance of the anode material. This report authenticates that Ce and Co co-doped SnSb can serve as an effective negative electrode for Li-ion batteries.

## Synthesis of anode materials

Tin-antimony nanoparticles were prepared by the simple coprecipitation technique. Stoichiometric amounts of metal chlorides of tin and antimony and tri-sodium citrate were dissolved in 40 ml distilled water. Following thorough mixing, this solution was reduced by the solution, which contains  $\text{NaBH}_4$  and  $\text{NaOH}$  reducing agents. Vigorous stirring of this mixture resulted in SnSb precipitates in the mixture solution. This precipitate was collected and washed with  $\text{HCl}$ , acetone, and distilled water, respectively. Co and Ce dopants were introduced into the metal chloride solution during the synthesis of SnSb:Ce, Co. All the remaining steps were followed as mentioned in the SnSb synthesis. The obtained precipitates were collected and used for further analysis.

These powders were tested for structural analysis (Panalytical XPertPro with  $\text{Cu-K}\alpha$  radiation), electrochemical analysis, and impedance analysis (Bio-Logic, SP-150). For impedance analysis, the samples were made into circular pellets (0.8-cm diameter and 1-mm thickness) and coated with Ag paste on both sides for electrical contact. The results obtained are discussed in the following sections.

## Electrode preparation

SnSb and doped electrodes were fabricated with an active material, an acetylene black conductor, and a PVdF binder with a weight ratio of 85:10:5 and mixed thoroughly to form slurry using *N*-methyl-2-pyrrolidone solvent. The slurry was coated onto a copper current collector with an apparent area of  $1 \text{ cm}^2$  and dried at  $100 \text{ }^\circ\text{C}$  for 24 h for solvent evaporation.

Electrochemical lithium insertion/extraction reactions of the tin-antimony were investigated by cyclic voltammetry. Electrochemical measurements were carried out using a three-electrode setup. The counter and reference electrodes were platinum electrode and saturated calomel electrode, respectively. The electrolyte solution used in this study was aqueous  $\text{LiNO}_3$ . The cyclic voltammetry was performed at room temperature for the pristine and doped tin-antimony. The potential window chosen for the analysis was within the stability range of the electrolyte (1.22 V) to avoid the  $\text{O}_2/\text{H}_2$  generation.

## Results and discussion

The phase compositions of the tin-based compounds are characterized by X-ray diffraction with  $\text{Cu (K}\alpha)$  radiation. The XRD pattern of pristine and doped SnSb powders in Fig. 1a illustrates the good crystallinity and pure phase of the alloy. All intense peaks are well indexed to the rhombohedral structure (space group  $R\bar{3}m$ ), and the parameters arrived from crystal structure data are listed in Table 1. The results are comparable with the standard JCPDS Card No. 33-0118, and there are no evident signals of impurity detected, which predicates the phase purity of the synthesized powders. There is no variation observed in the average particle size calculated from the Scherrer formula. The values are found to be 20 and 21 nm for SnSb and SnSb:Ce, Co, respectively. The volume of the unit cell is found to be similar for both the crystal systems, which is shown in Table 1. Here, the size of the dopant material Ce is higher than that of the parent element Sn. Hence, wobble structure formed in the pure SnSb contradicts

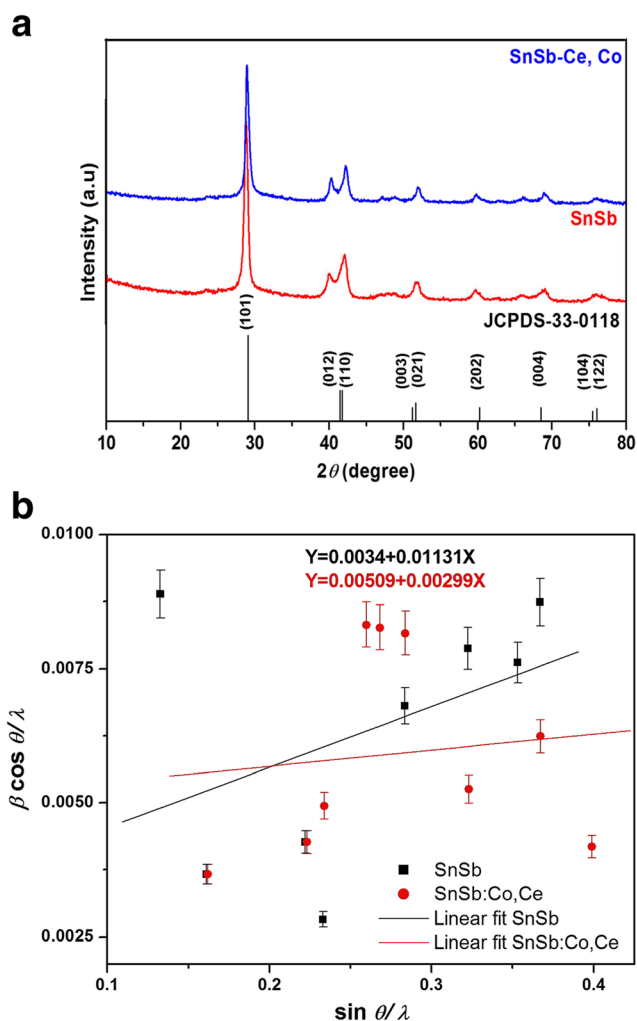


**Fig. 1** a XRD pattern of SnSb and SnSb:Ce, Co. b WH p/o analysis of SnSb and SnSb:Ce, Co

**Table 1** Lattice parameters calculated from XRD for SnSb and SnSb:Ce, Co JCPDS:  $c = 5.34$ ,  $a = 4.32$ ,  $V = 86.60 \text{ \AA}^3$ , and  $c/a = 1.23$ 

Sample	Crystallite size (nm)	Strain		$c$	$a$	$c/a$	Volume ( $\text{\AA}^3$ )
		$\varepsilon = \beta / \cot \theta$	WH plot				
SnSb	20.01	0.004502	0.01131	5.28	4.42	1.19	89.80
SnSb:Ce, Co	20.98	0.004361	0.00299	5.28	4.40	1.20	88.50

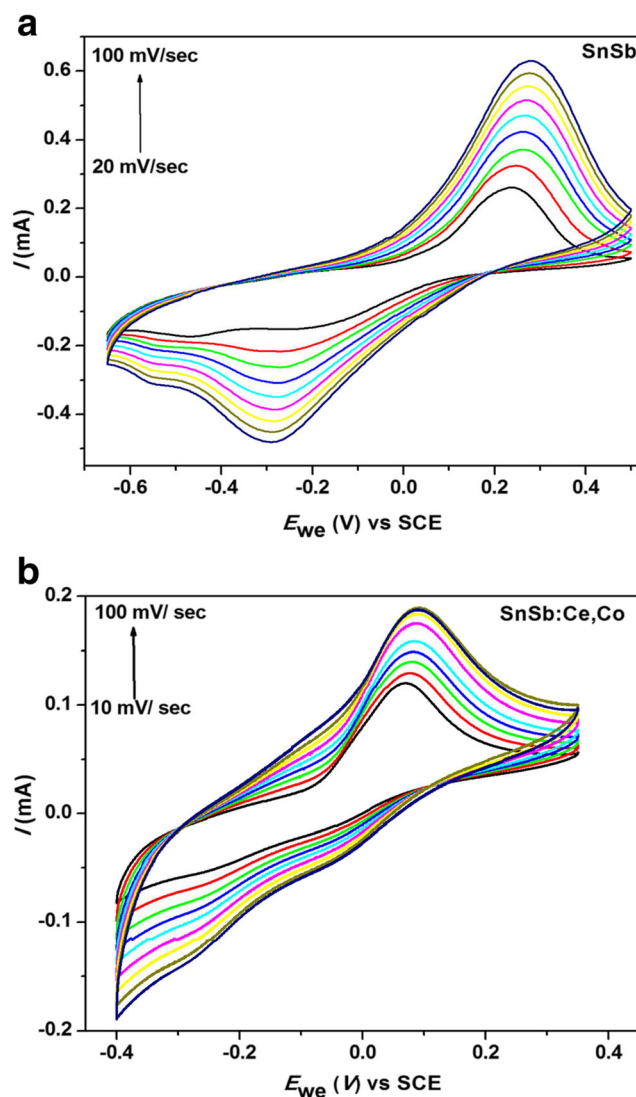
after doping with bigger ions. However, the percentage of dopant is very stumpy, which does not increase the volume of the unit cell. It attests that unit cell attains rigidity and the distance between atoms maybe decreased. This makes the electronic movement straightforward in between the atoms.

The orientations of (101), (012), and (202) peaks have shifted by  $0.11^\circ$  to the higher angle side. The shift to the higher angle side can be correlated either to the shrinkage of unit cell or in turn to the increase in internal stress in the lattice. This shift can be correlated to the decrease in the lattice parameter, which in turn indicates a volume reduction of the unit cell. As the  $d$ -spacing value for SnSb:Ce, Co is ( $-0.02 \text{ \AA}$ ) lesser than that of pristine SnSb, shrinkage of lattice in the previously said orientations is quiet possible. Size-induced and strain-induced broadening of XRD peaks can be analyzed using the Williamson-Hall (WH) plots. The WH graphical method is employed for estimating lattice strain. In WH plot, the plot between  $\beta \cos \theta$  and  $\sin \theta$  gives a straight line [31]. The linear fitted data (straight line) yield the slope and a constant. From the slope of the straight line, the strain gradient can be found. Figure 1b shows the WH plot analyzed for  $\text{Sn}_2\text{Sb}_3$  and  $\text{Sn}_1\text{Sb}_3\text{Co}_{0.5}\text{Ce}_{0.5}$  alloys. The linear fitted data give Y-intercept and slope of the straight line. The equation of the straight line is shown in Fig. 1b in which crystallite can be estimated from the Y-intercept and strain induced is obtained from the slope value of the straight line. The calculated values are compared with values obtained from other blueprints in Table 1.

The decrement in strain values on doping the Co and Ce in the pure SnSb is observed. The increment of lattice constants for the pure SnSb sample from the standard value points towards that tensile stress is developed in the synthesized samples, which increase the volume of the unit cell. However, the strain is minimized in the doped sample comparing the pure one, which indicates that unit cell contracts and hence the volume is minimized to some extent. The  $c/a$  ratio values are similar for both the samples; still, they deviate from the experimental  $c/a$  value which says that atoms are compressed along the  $c$ -axis of the rhombohedral unit cell. In the XRD pattern, the shifts of (101) and (012) peaks are evident for this. Also, corresponding  $d$ -values are found to decrease in these planes for doped samples compared to the pure SnSb. It shows that the atoms in the unit cell arrange in a more closed manner with dopants because of their larger ionic radii, and it indicates

that unit cell has achieved more stability. The rigid structure achieved with dopants provides the structural stability during the electrochemical reactions of the material. In precise, SnSb anode provided with Ce, Co dopants can withhold its structure during the charging/discharging process.

The redox behavior of the pristine and doped samples has been analyzed by cyclic voltammetry at various scan rates, and the results are shown in Fig. 2a, b, respectively. Alloying/de-alloying process of Li into and from the SnSb crystal structure is observed in between  $-0.5$  and  $0.5$  V. However, increased activity of the doped sample shifts the redox potentials and minimizes the operating potential window to  $-0.4$  to  $+0.4$  V. The oxidation peaks were recorded at  $-0.06$  and  $0.25$  V, and the corresponding reduction peaks were observed at  $0.02$  and  $-0.30$  V. These two pairs of redox behavior obtained for both the

**Fig. 2** a CV analysis of SnSb for different scan rates. b CV analysis of SnSb:Ce, Co for different scan rates

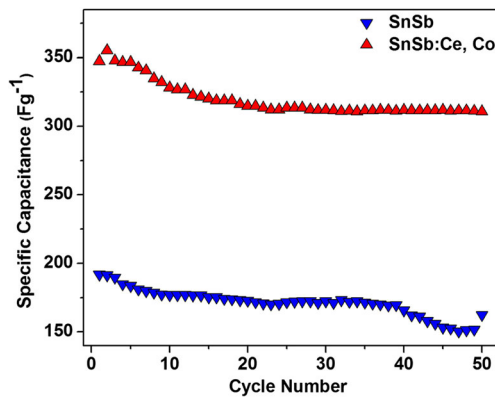


**Fig. 3** Specific capacitance of SnSb and SnSb:Ce, Co

samples indicate the alloy formation of Sn/Li and Sb/Li during electrochemical activity. Since the employed dopants Ce and Co in the present system are inactive in

redox activity, no additional redox peaks are observed in the doped sample. But structural refinement produces well-resolved reduction behavior in the SnSb:Ce, Co. As the working potential window is altered, this significantly produces variation in the redox peak. Hence, doping with Ce and Co alters the redox activity of the system. Quantitative assessment of charge storage capacity of the SnSb alloy nanoparticles can be made by means of the specific capacitance estimation from cyclic voltammetry. As the anodic and cathodic curves are not similar in cyclic voltammetric results, the sum of these curves can be used for representing voltammetric charges in specific capacitance calculation. The specific capacitance is computed accurately using the formula

$$C = \int_{E1}^{E2} i(E) dE / 2(E2 - E1)mv$$

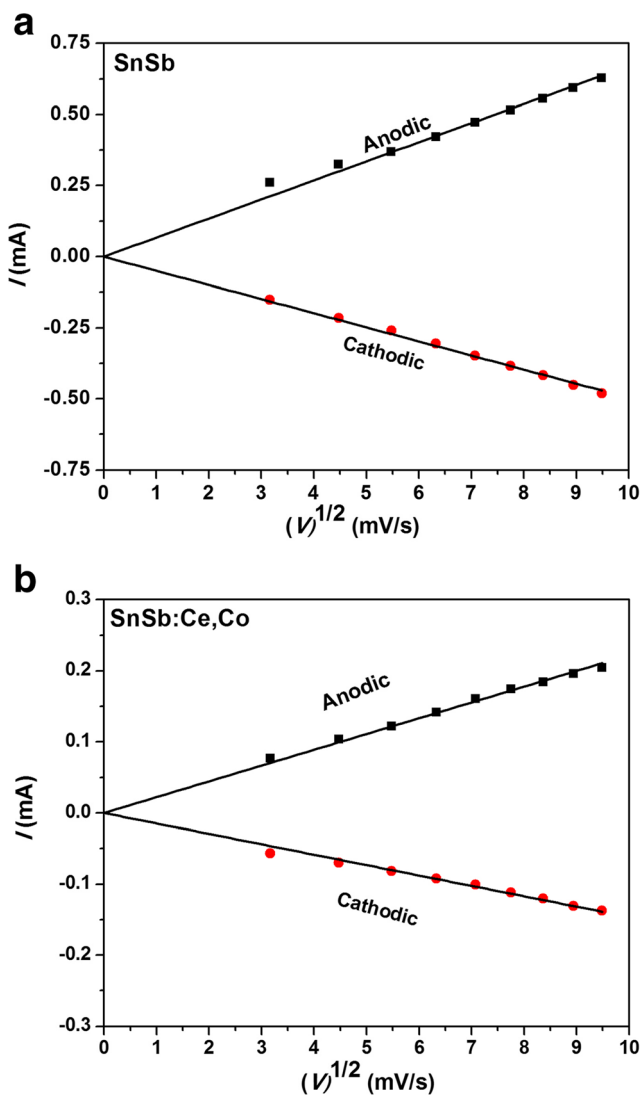


**Fig. 4** **a** Plot of scan rate vs peak current for SnSb. **b** Plot of scan rate vs peak current for SnSb:Ce, Co

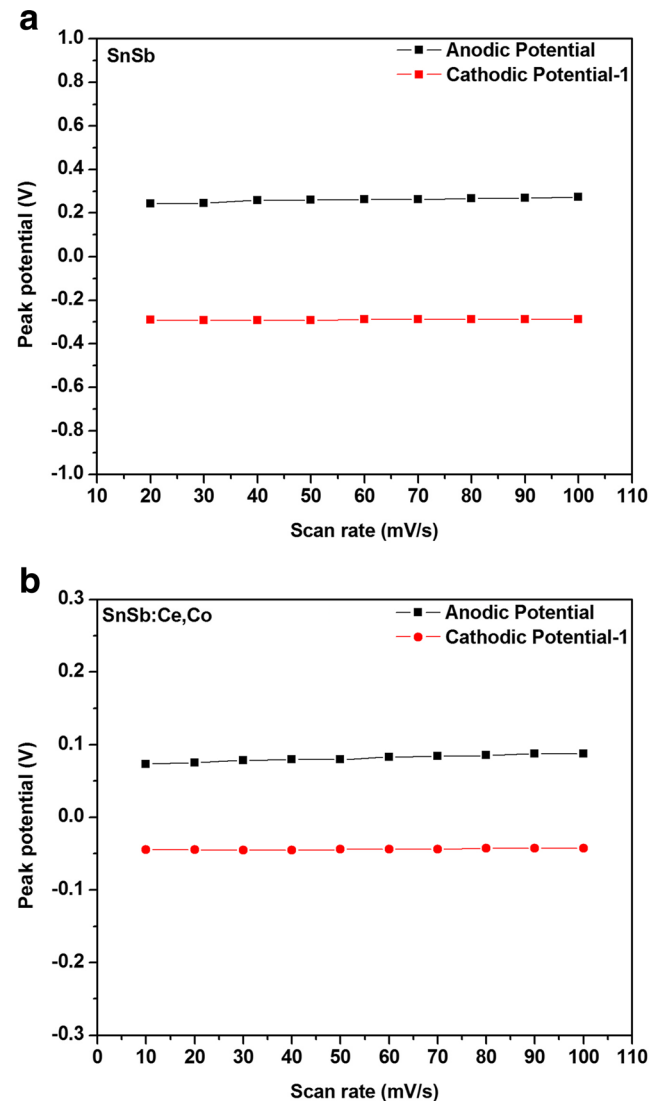


**Fig. 5** **a** Plot between scan rate and peak potential SnSb. **b** Plot between scan rate and peak potential SnSb:Ce, Co

**Table 2** Electrochemical parameters calculated from CV for SnSb and SnSb:Ce, Co samples

Sample	Scan rate (mV s <sup>-1</sup> )	$\Delta E_p$ (mV)	$i_{pc}/i_{pa}$	$D \times 10^{-11}$ (cm <sup>2</sup> s <sup>-1</sup> )	
				Anodic	Cathodic
SnSb	20	417	0.5	1.79	1.57
SnSb:Ce, Co		323	0.7	1.34	2.55

where,  $\int_{E_1}^{E_2} i(E)dE$  is the integrated area of the instantaneous current over the range of cutoff potentials  $E_1$  and  $E_2$ . ( $E_2 - E_1$ ) is the working potential window of the electrochemical system,  $m$  is the mass of the working electrode in grams, and  $v$  is scan rate in volts per second.

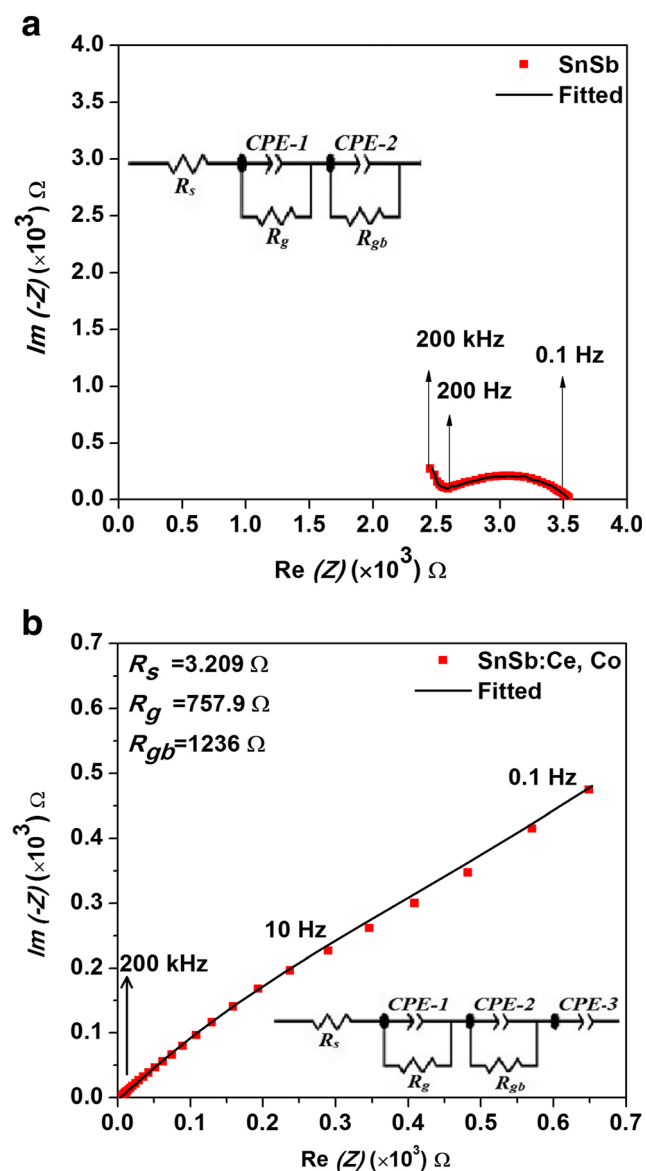


**Fig. 6** a Nyquist plot of SnSb. b Nyquist plot of SnSb:Ce, Co

The estimated values of specific capacitance over 50 cycles are shown in Fig. 3. The SnSb exhibits specific capacitance 176 Fg<sup>-1</sup>, and doped sample shows 319 Fg<sup>-1</sup>, which is 81.25 % higher than that of pure SnSb. It is clear that capacity enhancement is achieved with the addition of dopants into the pure SnSb together with the stable specific capacitance over 50 cycles. Consequently, the addition of inactive dopants buffers the volumetric change during the electrochemical activity of neat SnSb anode and constant specific capacitance is achieved over more number of cycles. However, these values are lower than the theoretical capacity of the pure SnSb anode (962 mAh g<sup>-1</sup>), and experimental capacity reported by other researchers [32]. The resulted low capacitance value could possibly be due to the chosen aqueous-based system for testing reversibility, which is available in the laboratory.

A Nernstian system (reversible electrochemical system) is expected to possess the following characteristics such as unit value of peak current ratio, potential

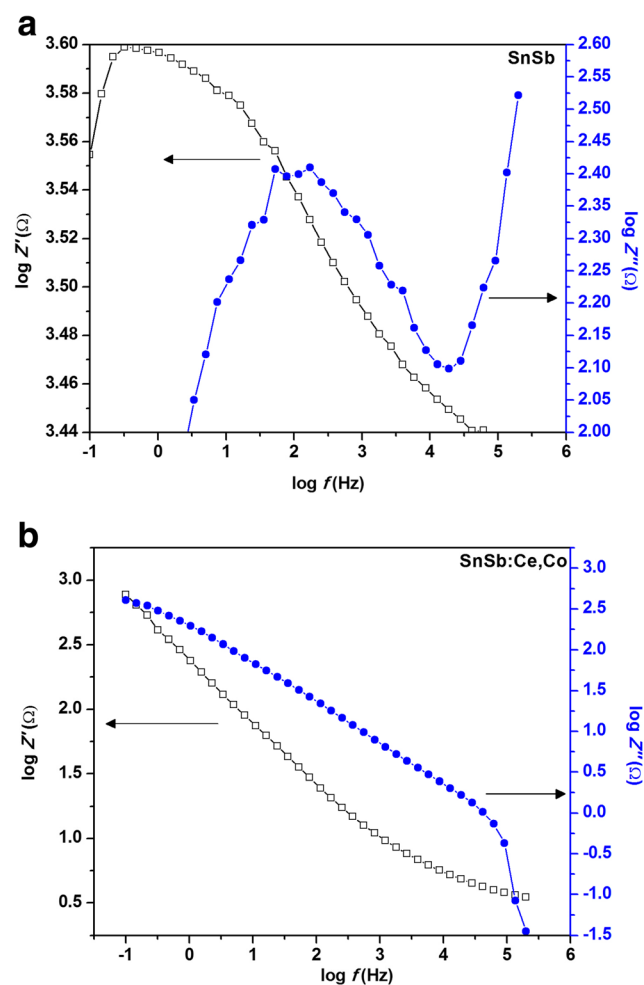
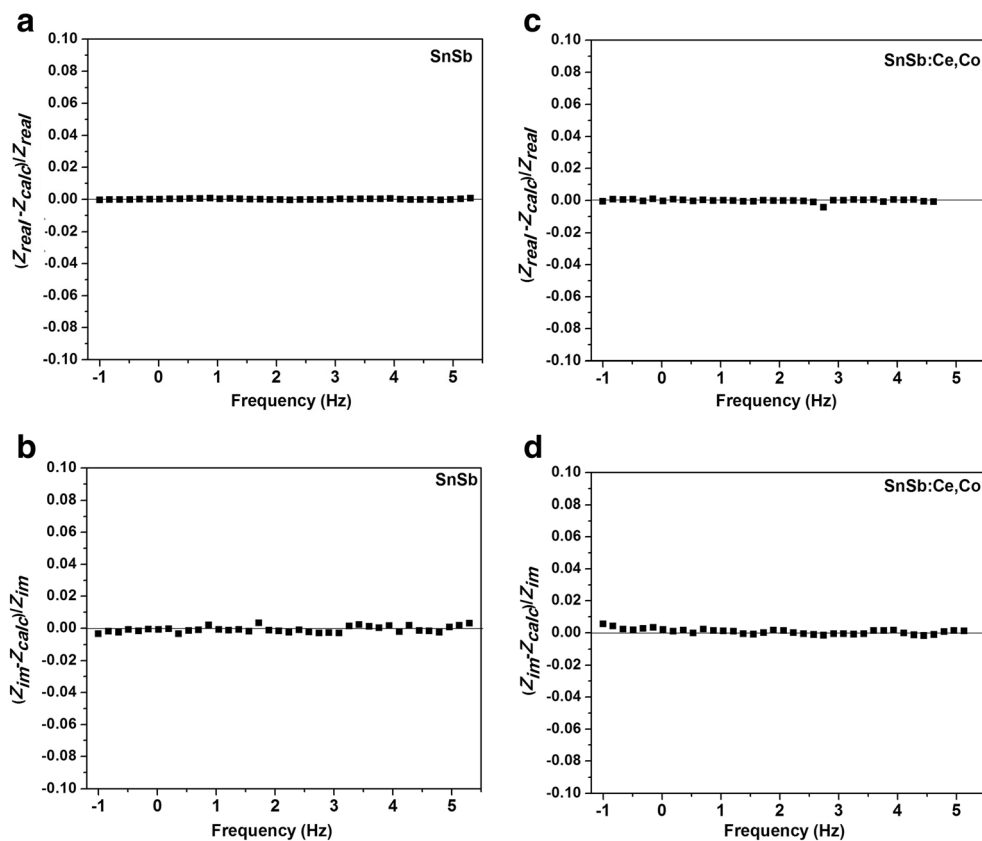


**Fig. 7** a Bode plot of SnSb. b Bode plot of SnSb:Ce, Co

difference between oxidation and reduction peak around 59 mV, and linear behavior between peak current and square root of scan rate. Reviewing all these phases clearly indicates that the chosen electrochemical system for SnSb and SnSb:Ce, Co exhibits slight deviation from the standard reversible nature, which can be ascribed as the quasi reversibility of the system. The plot between the square root of scan rate and peak current values is shown in Fig. 4a, b for SnSb and SnSb:Ce, Co samples. Also, independency of peak potential with different scan rates is verified in Fig. 5a, b ensuring the reversibility of the system. As diffusion co-efficient ( $D$ ) values are related to the charge transfer kinetics of the electrochemical system, these are calculated using the Randles-Sevcik equation and the values are displayed in Table 2. The obtained  $D$  values are higher than the values reported by other researchers for LiSn lithiated phase [33]. Hence, SnSb alloy synthesized with Ce and Co dopants can be effectively used as the anode material for Li-ion batteries. Conductivity analysis is made for both the samples in the frequency range of 100 mHz to 100 kHz at room temperature. The impedance of the real part vs. imaginary part is shown in Nyquist plot (shown in Fig. 6a, b) for both the materials. The equivalent circuit which fits the impedance behavior of the SnSb and

SnSb:Ce, Co alloys is shown in the inset of respective plots. Nyquist plot of these samples shows the depressed semicircle which reflects the distribution of relaxation time. Further understanding can be clearly focused using the frequency-dependent impedance behavior, i.e., Bode plots (Fig. 7a, b). The broad impedance peaks observed vs. frequency show the non-Debye relaxation phenomena in the present samples, and this can be correlated with different effects such as grain, grain boundary, and electrode-electrolyte surface. Comparing the Bode plots of SnSb and SnSb:Ce, Co samples, the grain region (generally observed at higher frequency) is not altered to a greater extent. However, the grain boundary component (observed at intermediate/high-frequency region) does not show any relaxation processes in the measured frequency region. As discussed earlier in structural analysis, the dopant atoms involve a strain in the unit cell. Further, in addition to frequency vs. impedance representation, the compliance of causality, linearity, and stability is ensured in the measurement by means of residual/error analysis [34]. The error analyses stand as a proof for the validation of impedance fit parameters obeying the Kramers-Kronig relations (Fig. 8a–d). The residual plots of SnSb and SnSb:Ce, Co in both real and imaginary values over the measured frequency region show minor

**Fig. 8** **a** Error analysis for real  $z$  vs frequency of SnSb. **b** Error analysis for  $im(-z)$  vs frequency of SnSb. **c** Error analysis for real  $z$  vs frequency of SnSb:Ce, Co. **d** Error analysis for  $im(-z)$  vs frequency of SnSb:Ce, Co



noise ( $\sim 10^{-4}$  %), which satisfies the causality, linearity, and stability criteria during the impedance measurement offering reliability on the measurements. The fit parameters calculated from the experimental data are shown in Table 3. The capacitance values of the different regions, as calculated from the values of fit parameters using the formula [35]

$$C = \frac{(Q^*R)^{1/n}}{R}$$

where

- C Capacitance (F)  
 Q Constant phase element ( $s^{-n}$ )  
 R Resistance ( $\Omega$ )  
 N Exponent value

show that these components correspond to the grain and grain boundary regions in the SnSb and SnSb:Ce, Co alloy samples under investigation [36]. The calculated values of electrical conductivity for the grain and grain boundary components are listed in Table 3. From Table 3, it is clear that the capacitance of grain has decreased in turn resulting in higher conduction on doping. Similarly, grain boundary conduction has increased, which is quiet favorable for application, but a mild increase in the capacitance is a playoff. On the whole, due to the doping of Ce and Co atoms into the SnSb matrix, the mobility gets enhanced, which results in improved electrical conductivity. Such a behavior is desired when the anode is expected to exhibit higher rate capability. Also, the electrochemical behavior and capacitance of the parent anode material have been augmented while it is provided with dopants. Hence, the material SnSb:Ce, Co is expected to perform as an efficient anode in the Li-ion battery systems. However, the

stability of the anode against organic electrolyte and solid electrolytes is the interest of future work.

## Conclusion

Ce and Co co-doped tin-antimony anodes are prepared and analyzed for various properties. Even with dopants, rhombohedral structure of SnSb is preserved. Addition of dopants buffers the volumetric changes of the SnSb alloy during lithiation and de-lithiation process of SnSb anode, which leads to increased specific capacitance and stability over higher number of cycles for the doped SnSb compared to the pristine. Electrical conductivity is in similar order for the SnSb:Ce, Co as of the pure sample. Hence, SnSb:Ce, Co can be used as an effectual negative electrode in the Li-ion batteries which can preserve the structure from disintegration over more number of charge/discharge cycles.

**Acknowledgments** One of the authors, D. Lakshmi, acknowledges DST-INSPIRE fellowship (no. IF130640) for the financial support under AORC scheme. One of the authors, Dr. B. Nalini, gratefully acknowledges BRNS (no. 2012/37C/32/BRNS) for the financial aid.

## References

1. Wu FD, Wu M, Wang Y (2011) *Electrochem Commun* 13:433–436
2. Ferguson PP, Todd ADW, Dahn JR (2010) *Electrochem Commun* 12:1041–1044
3. Lee JM, Chang WS, Yu BC, Kim H, Im D, Doo SG, Sohn HJ (2010) *Electrochem Commun* 12:928–932
4. Qiu C, Yuan Z, Liu L, Ye N, Liu J (2012) *J Solid State Electrochem* 17:841–847
5. Ren J, He X, Wang L, Pu W, Jiang C, Wan C (2007) *Electrochim Acta* 52:2447–2452
6. Kepler KD, Vaughey JT, Thackeray MM (1999) *Electrochem Solid State Lett* 2:307–309
7. Ke FS, Huang L, Cai JS, Sun SG (2007) *Electrochim Acta* 52:6741–6747
8. Yang J, Takeda Y, Imanishi N, Yamamoto O (1999) *J Electrochem Soc* 146:4009–4013
9. Poizot P, Laruelle S, Grugeon S, Dupont L, Tarascon JM (2000) *Nature* 407:496–499
10. Cabana J, Monconduit L, Larcher D, Palacin MR (2010) *Adv Mater* 22:E170–E192
11. Dey AN (1971) *J Electrochem Soc* 118:1547–1549
12. Kasavajjula U, Wang C, Appleby AJ (2007) *J Power Sources* 163:1003–1039
13. Chan CK, Zhang XF, Cui Y (2008) *Nano Lett* 8:307–309
14. Park MH, Cho Y, Kim K, Kim J, Liu M, Cho J (2011) *Angew Chem Int Ed* 50:9647–9650
15. Seng KH, Park MH, Guo ZP, Liu HK, Cho J (2012) *Angew Chem Int Ed* 51:5657–5661
16. Wang J, Du N, Zhang H, Yu J, Yang D (2012) *J Mater Chem* 22:1511–1515
17. Courtney IA, Dahn JR (1997) *J Electrochem Soc* 144:2045–2052
18. Idota Y, Kubota T, Matsufuji A, Maekawa Y, Miyasaka T (1997) *Science* 276:1395–1397

**Table 3** Fit parameters and room temperature conductivity values of SnSb and SnSb:Ce, Co samples

Sample	SnSb	SnSb:Ce, Co
Rs	6.209	3.163
Rg	1055	747.6
Rgb	2508	1307
CPE-g	$0.2533 \times 10^{-9}$	$7.13 \times 10^{-9}$
n	0.8679	0.5630
CPE-gb	$1.5229 \times 10^{-6}$	$0.2895 \times 10^{-6}$
n	0.5229	0.7426
C-g	$25.53 \times 10^{-12}$	$0.5763 \times 10^{-12}$
C-gb	$9.472 \times 10^{-9}$	$18.857 \times 10^{-9}$
$\sigma_g$ (S cm <sup>-1</sup> )	$3.7915 \times 10^{-4}$	$5.2777 \times 10^{-4}$
$\sigma_{gb}$ (S cm <sup>-1</sup> )	$1.5948 \times 10^{-4}$	$3.2362 \times 10^{-4}$

19. Dahn JR, Mar RE, Abouzeid A (2006) *J Electrochem Soc* 153: A361–A365
20. Trahey L, Vaughey JT, Kung HH, Thackeray MM (2009) *J Electrochem Soc* 156:A385–A389
21. Nithyadharseni P, Reddy MV, Nalini B, Saravanan P, Vinod VTP (2016) Miroslav Čemik, Chowdari BVR. *J Solid State Electrochem* 20:1743–1751
22. Chen S, Archer LA, Lou XW (2011) *J Mater Chem* 21:9912–9924
23. Yan J, Sumboja A, Khoo E, Lee PS (2011) *Adv Mater* 23: 746–750
24. Kim MG, Cho J (2009) *J Electrochem Soc* 156:A277–A282
25. Yang J, Takeda Y, Imanishi N, Ichikawa T, Yamamoto O (1999) *J Power Sources* 79:220–224
26. Dawei , Bonan, Beibei, Zhang, Qiang, Ru, Xianhua, Hou, Shejun, Hu (2014) *J Solid State Electrochem* 18:2573–2579
27. Winter M, Besenhard JO (1999) *Electrochim Acta* 45:31–50
28. Stjern Dahl M, Bryngelsson H, Gustafsson T, Vaughey JT, Thackeray MM, Edström K (2007) *Electrochim Acta* 52:4947–4955
29. Tamura N, Fujimoto M, Kamino M, Fujitani S (2004) *Electrochim Acta* 49:1949–1956
30. Nithyadharseni P, Reddy MV, Nalini B, Kalpana M, Chowdari BVR (2015) *Electrochim Acta* 161:261–268
31. Vives S, Gaffet E, Meunier C (2004) *Mater Sci Eng A* 366: 229–238
32. Ru Q, Tian Q, Hu S, Zhao L (2011) *Int J Miner Metall Mater* 18: 216–222
33. Nitta N, Yushin G (2014) *Part Part Syst Charact* 31:317–336
34. Pankaj A, Crisalle OD, Orazem ME (1995) *J Electrochem Soc* 142(12):4149–4158
35. Hirschorn B, Orazem ME, Tribollet B, Vivier V, Frateur I, Musiani M (2010) *Electrochim Acta* 55:6218–6227
36. Irvine John TS, Sinclair Derek C, West Anthony R (1990) *Adv Mater* 2(3):132–138